Electronic Supplementary Material

Synthesis of micro- and nanosheets of $CrCl_3$-$RuCl_3$ solid solution by chemical vapour transport

Samuel Froeschke, Daniel Wolf, Martin Hantusch, Lars Giebeler, Martin Wels, Nico Gräßler, Bernd Büchner, Peer Schmidt and Silke Hampel

S1 Additional information regarding CVT experiments

Purification of starting material

For the purification CVT of $CrCl_3$, it is possible to perform a cleaning transport with an inverse temperature gradient (source: 700 °C, sink: 800 °C) before the actual transport. This is not possible for the $RuCl_3$ transport since there an exothermal transport of Ru is occurring.

In case of a chlorine deficit during the $CrCl_3$ transport (e.g. $CrCl_2$ impurities), a sequential transport of $CrCl_2$ starts after the $CrCl_3$ depletion in the source. In this case the purification transport needs to be stopped before all of the $CrCl_3$ in the source is depleted, otherwise grey $CrCl_2$ will contaminate the $CrCl_3$ in the sink, as shown in Figure S1 (a).

In the case of the purification of commercial $RuCl_3$ powder (which often contains significant contaminations oxygen or water) the transport also must be stopped before the $RuCl_3$ in the source is depleted. Otherwise the sequential transport of RuO_2 will start, resulting in the contamination of the previously purified $RuCl_3$ in the sink. If this happens, we observed the formation of a black ring-like deposition in the sink of the ampoule, as seen in Figure S1 (b). Another indication of already started RuO_2 transport is the absence of black $RuCl_3$ crystals in the source. Also note, that (depending on the amount of oxygen and water contamination of the starting material) a significant amount of chlorine might be released inside the ampoule during the experiment, which can build up high pressures. Most of the released chlorine will remain gaseous even after slow cooling to room temperature, which can sometimes be observed by a slight green colour of the ampoule atmosphere. Before opening the ampoule, we strongly advised to condense the chlorine in the ampoule, otherwise the pressure inside can cause an explosion when opening the ampoule.

Growth of micro- and nanocrystals

A cleaning transport for the substrate experiments with solid solution starting material is not possible, because of an exothermal Ru transport. When taking the ampoule out of the furnace after the desired transport duration, we advise to first quench the source side of the ampoule in cold water before quenching the hole ampoule to avoid condensation of vapour on the substrate.

S2 Details about EDX quantification

To increase the precision of the EDX quantification results, the synthesized solid solution samples with known composition (weighed ratio from synthesis) were used as external standards for the calibration of Cr-K-, Cl-K- and Ru-L-lines over the whole composition range by averaging 5 measurements for each sample. The analysis of crystals grown on substrates was conducted by measuring 5 random crystals on the substrate and averaging the results. The quantification was done by utilising the external standard sample with the composition closest to the actual sample, e.g. external standard sample of $x = 0.4$ for actual samples with $0.35 \leq x < 0.45$.

S3 Additional information regarding thermodynamic simulations

For the simulations and calculations of the CVT we used $\Delta H_f°$, $S°$ and the $C_p°$-function of known condensed and vapour species in the element system Cr-Ru-Cl-O-H-Ar, since we performed the simulations with traces of water, which might be released during the

Figure S1 – (a) Image of the ampoule after $CrCl_3$ purification transport with Cl deficit. The transport duration was chosen too long, so that also grey $CrCl_2$ was transported and deposited (marked in red). (b) Black RuO_2-ring that forms during the purification transport of commercial $RuCl_3$ powder, when all $RuCl_3$ in the source is depleted and the sequential transport of RuO_2 takes place.

experiment by the ampoule or is adsorbed on the surface (and Ar traces remaining from the glovebox atmosphere). The thermodynamic data we used for the simulations are stated in the Table S1 and Table S2. In addition to the species stated there, we also investigated the influence of some other species, which were not used for further simulations due to instability or to low partial pressures. The used thermodynamic data of those species is not stated here.

The additionally investigated vapour species were as follows: O_3, OH, HO_2, H_2O_2, ClO, ClO_2, ClO_3, Cl_2O, Cl_2O_2, HOCl, Cr, Cr_2, CrH, CrO, CrO_2, CrO_3, Cr_2O, Cr_2O_2, CrOH, $Cr(OH)_2$, CrO_2OH, $CrO(OH)_2$, $Cr(OH)_3$, $CrO_2(OH)_2$, $CrO(OH)_3$, $Cr(OH)_4$, $CrO(OH)_4$, $Cr(OH)_5$, $Cr(OH)_6$, CrOCl, CrO_2Cl, CrO_2Cl_2, RuO, RuO_2, RuO_3, RuO_4, RuOH, $Ru(OH)_2$

The additionally investigated condensed species were as follows: Cr (l), CrO (l), CrO_2, CrO_3, CrO_3 (l), Cr_2O_3 (l), $Cr(CrO_4)$, $Cr(CrO_4)$ (l), $Cr_2(CrO_4)_3$, $Cr_3(CrO_4)_3$ (l), Cr_3O_4, Cr_8O_{21}, $Cr(OH)_2$, CrO_2Cl_2 (l), Ru (l), RuO_4, RuO_4 (l)

To simulate the CVT behaviour of the solid solution, we modified the latest published version 5.1 of the software TRAGMIN[1]. Doing so, we enabled the use of more complex C_p-functions up to 8 parameters with flexible temperature exponent. Also, we extended the software to allow for a use of gapless solid solution compositions. For our calculations we assumed ideal solid solution formation without any enthalpy of mixing, whereas the mixing entropy is calculated as follows[2]:

$$\Delta_{mix}S^\circ = x \cdot R \cdot \ln(x) + (1-x) \cdot R \cdot \ln(1-x) \tag{S1}$$

The most important chemical equilibria reactions where extracted from the calculated transport efficiencies, shown in Figure S2. Comparing the summed-up efficiencies of the Ru-species at the different mean temperatures, one can see that at the higher temperature (dashed line) the summed-up efficiencies of the Ru-species are higher compared to the ones at the lower temperature (solid line), while all efficiencies are normalized on the summed efficiencies of the Cr-species. This means that the chromium chloride enrichment for the solid solution deposition should decrease when increasing the mean temperature from 550 °C to 625 °C.

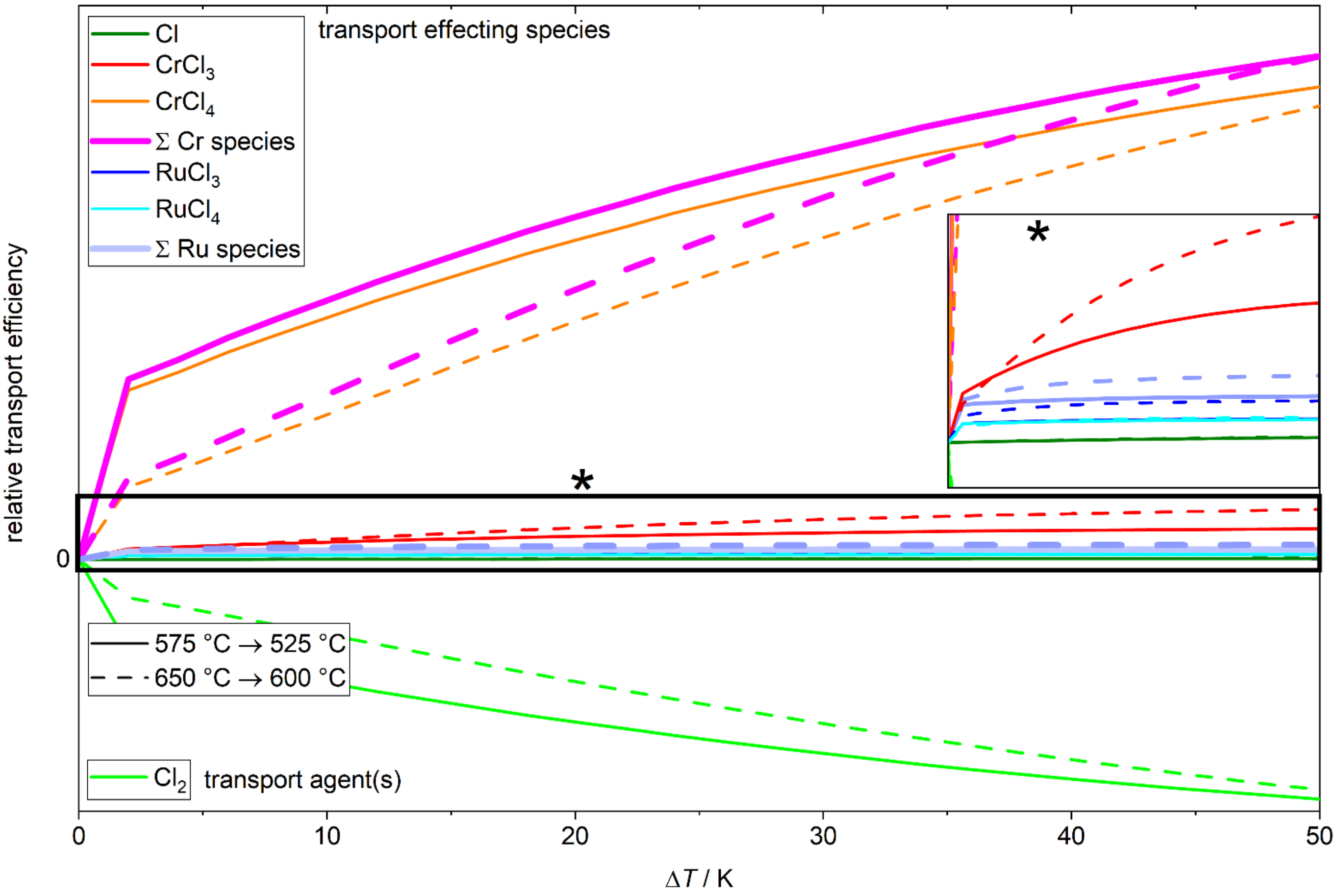

Figure S2 – Calculated transport efficiencies for the CVT of a $Cr_xRu_{1-x}Cl_3$ sample with $x = 0.5$ for a transport from 575 °C ⇨ 525 °C (solid lines) and 650 °C ⇨ 600 °C (dashed line). The stronger lines are the sums of the Cr-species and Ru-species respectively. The area of efficiencies with low absolute values is magnified at an insert picture for better distinction between different species. The efficiencies for each temperature are normalised to the summed maximum value of the Cr-species to allow comparison of the magnitude of predicted enrichment at the different temperatures.

Table S1 – Thermodynamic data of vapour species used for simulations. *

species	reference	T_{ref} / K	$\Delta H_f°$ / J·mol^{-1}	$S°$ / J·(mol·K)$^{-1}$	*a*	*b*	*c*	*d*	*e*	*f*	*g*
Ar	FactPS	298	0.000	154.845	20.786						
Cl	FactPS	298	121.302	165.189	26.529	-3.103			-1125.572		
	FactPS	600			24.067		-17.534		9269.508	-282.155	-0.014
Cl_2	FactPS	298	0.000	223.079	20.681		3.167		-8299.370	591.261	0.191
Cl	FactPS	298	-92.312	186.901	13.384	17.309	-6.231	-3.803	5347.397		
H	FactPS	298	218.000	114.717	20.786						
H_2	FactPS	298	0.000	130.680	19.826	3.078	-2.952	1.430		194.861	
	FactPS	1200			14.387	2.064	208.332		-74353.404	2134.835	
O	FactPS	298	249.173	161.058	19.965	0.264	0.587	-0.037		20.952	
O_2	FactPS	298	0.000	205.147	26.924	16.979	2.293	-6.766		-79.162	
	FactPS	1000			89.681	-1.447	-186.827		95803.960	-4126.537	
H_2O	FactPS	298	-241.826	188.832	28.409	12.475	1.283	0.361			
	FactPS	1100			31.430	14.111	-24.926	-1.833			
CrCl	FactPS	298	129.900	249.790	36.449	1.724	-1.793	-0.859			
	FactPS	1000			45.553	-8.315	-25.136	2.383			
$CrCl_2$	FactPS	298	-117.600	319.469	60.993	-4.937	-0.653	2.438			
	FactPS	1000			59.654	-1.308	-0.003	0.322			
$CrCl_3$	FactPS	298	-283.000	347.030	94.475	-17.113	-6.880	7.506			
	FactPS	1000			85.199	-1.784	2.862	0.443			
$CrCl_4$	FactPS	298	-396.500	371.920	120.435	-13.251	-12.952	3.933			
	FactPS	1000			110.429	-1.662	7.514	0.350			
$CrCl_5$	FactPS	298	-389.600	407.160	139.521	0.647	-14.951	-3.947			
	FactPS	1000			135.281	-1.336	6.982	0.220			
$CrCl_6$	FactPS	298.	-345.300	414.950	154.615	6.046	-11.167	-3.031			
	FactPS	1000			157.938	0.022	-14.171	-0.004			
Cr_2Cl_4	[3]	298	-487.436	473.210	128.620	128.620	-5.540				
$CrOCl_2$	FactPS	298	-336.500	333.030	88.368	-1.812	-10.748	-1.353			
	FactPS	1000			85.237	-1.517	1.570	0.326			
$CrOCl_3$	FactPS	298	-507.800	357.320	105.132	16.058	-14.110	-11.157			
	FactPS	1000			110.032	-1.157	-2.634	0.191			
$CrOCl_4$	FactPS	298	-517.600	369.350	119.708	22.417	-11.230	-10.732			
	FactPS	1000			132.686	0.202	-25.119	-0.033			
CrO_2Cl_2	FactPS	298	-519.200	329.530	85.606	37.557	-9.908	-17.886			
	FactPS	1000			116.867	-8.577	-62.502	2.298			
$RuCl_3$	[4] ($\Delta H_f°$ + $S°$)	298	16.900	363.700	80.840		2.747				
	FactPS (C_p)	800			54.800	11.490					
$RuCl_4$	[4] ($\Delta H_f°$ + $S°$)	298	-93.300	374.100	91.320		1.511				
	FactPS (C_p)	800			64.160	11.990					
RuOCl	[5]	298	90.016	201.385	54.428						

*C_p function defined as follows: $C_p° = a + b \cdot 10^{-3} \cdot T + c \cdot 10^{5} \cdot T^{-2} + d \cdot 10^{-6} \cdot T^{2} + e \cdot T^{-1} + f \cdot T^{-1/2} + g \cdot T^{1/2}$

If more than one T_{ref} is listed, the second value is the upper limit for the first $C_p°$-function and acts as T_{ref} for temperatures above. Blank entries for $C_p°$-parameters mean that this value is 0.

FactPS as source refers to literature [6].

Table S2 - Thermodynamic data of condensed species used for simulations. *

species	source	T_{ref} / K	$\Delta H_f°$ / J·mol^{-1}	$S°$ / J·(mol·K)$^{-1}$	a	b	c	d	e	f	g
Cr	FactPS	298	0.000	23.543	26.908	-3.789	-2.785	8.863			
$CrCl_2$	FactPS	298	-395.388	115.311	73.245	12.996	-5.288				
$CrCl_2$ (l)	FactPS	298	-365.952	142.108	73.245	12.996	-5.288				
	FactPS	900			100.416						
$CrCl_3$	FactPS	298	-544.400	122.900	84.916	32.074	-2.381				
$CrCl_3$ (l)	FactPS	298	-501.717	131.488	130.000						
Cr_2O_3	FactPS	298	-1127.120	84.771	121.440	7.800	-20.000				
Ru	FactPS	298	0.000	28.535	21.962	4.929	0.456	1.113			
$RuCl_3$	[4] ($\Delta H_f°$ + $S°$)	298	-221.200	153.300	159.500		-8.900			-988.700	
	FactPS (C_p)	600			91.980	41.220					
RuO_2	FactPS	298	-305.014	58.158	106.600		-17.520			-524.200	
	FactPS	900			73.580	15.150					

*C_p function defined as follows: $C_p° = a + b \cdot 10^{-3} \cdot T + c \cdot 10^{5} \cdot T^{-2} + d \cdot 10^{-6} \cdot T^{2} + e \cdot T^{-1} + f \cdot T^{-1/2} + g \cdot T^{1/2}$

If more than one T_{ref} is listed, the second value is the upper limit for the first $C_p°$-function and acts as T_{ref} for temperatures above. Blank entries for $C_p°$-parameters mean that this value is 0.

FactPS as source refers to literature [6].

S4 STA measurements

For the STA measurements, the sample and device were purged at 40 °C with Ar gas flow until stable conditions were reached. The increasing differential scanning calorimetry (DSC) signal up to about 520 °C is device related, while the change in trend at 520 °C is related to an actual reaction occurring in the sample. The start of the chemical reaction is indicated by a slight decrease in mass. Such mass loss can be explained by the starting sublimation in combination with marginal decomposition to Ru (s),

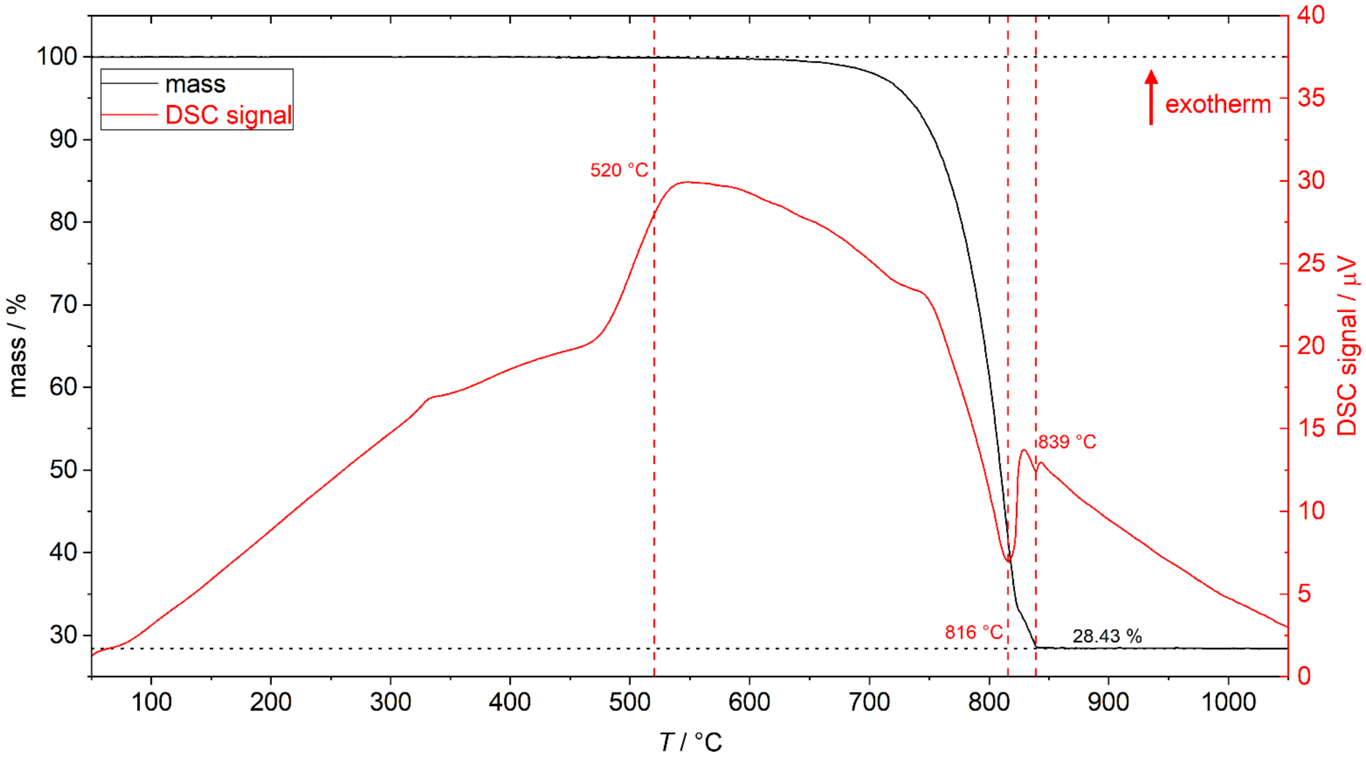

Figure S3 – STA measurement of a $Cr_{0.5}Ru_{0.5}Cl_3$ sample with important temperatures and masses marked.

whereas both processes are accelerated with increasing temperature. The step in the DSC signal and mass loss at 816 °C might mark the point, at which all $CrCl_3$ has been removed from the sample by sublimation, while a small portion of $RuCl_3$ is still remaining. Still, when the temperature reached 839 °C all the remaining $RuCl_3$ was removed or decomposed, leaving behind only elemental Ru (s), since the remaining 28.43 % of the total starting mass correspond very well with the mass faction of Ru in the starting composition of $Cr_{0.5}Ru_{0.5}Cl_3$ (theoretically 27.63 %). The deviation from this ideal value can be attributed to a slight deviation from a starting composition of $x = 0.5$ in combination with possible traces of Cr_2O_3 (s) formation due to oxygen traces in the system. Please note that the transport relevant reactions (1), (4) and (5) can only occur under equilibrium conditions in a closed reaction system (with temperature and thus site dependent forward and backward reaction). In contrast, during the STA experiments, the released Cl_2 due to decomposition reaction (2) is lost for the equilibrium and thus solid Ru remains.

S5 Additional pXRD data

Table S3 – Refined unit cell parameters of $Cr_{1-x}Ru_xCl_3$ samples.

x	a / Å	b / Å	c / Å	β / °	V / Å^3	interlayer distance / Å	$(a\sqrt{3})/b$
0 ($CrCl_3$)	5.958(6)	10.3328(20)	6.110(5)	108.522(15)	356.70(8)	5.794(4)	0.9988(17)
0.1	5.9586(21)	10.3254(8)	6.1063(19)	108.559(6)	356.153(27)	5.7887(16)	0.9995(6)
0.2	5.9605(16)	10.3296(6)	6.1014(15)	108.646(4)	355.941(21)	5.7811(13)	0.9994(5)
0.3	5.96465(25)	10.31824(9)	6.09893(25)	108.7076(7)	355.526(3)	5.77671(21)	1.00124(8)
0.4	5.9677(13)	10.3331(5)	6.0896(12)	108.743(4)	355.601(18)	5.7667(10)	1.0003(4)
0.5	5.9690(13)	10.3384(5)	6.0834(12)	108.793(4)	355.388(19)	5.7591(10)	1.0000(4)
0.6	5.9697(18)	10.3507(7)	6.0724(16)	108.780(5)	355.240(26)	5.7491(13)	0.9990(5)
0.7	5.9730(11)	10.3401(5)	6.0745(11)	108.839(3)	355.072(17)	5.7491(9)	1.0005(4)
0.8	5.9739(29)	10.3532(12)	6.0678(27)	108.850(8)	355.16(5)	5.7424(23)	0.9994(9)
0.9	5.9760(20)	10.3537(8)	6.0608(19)	108.919(6)	354.75(3)	5.7334(16)	0.9997(6)
1 ($RuCl_3$)	5.9731(5)	10.34606(21)	6.0385(5)	108.8314(14)	353.191(7)	5.7152(4)	0.99997(16)

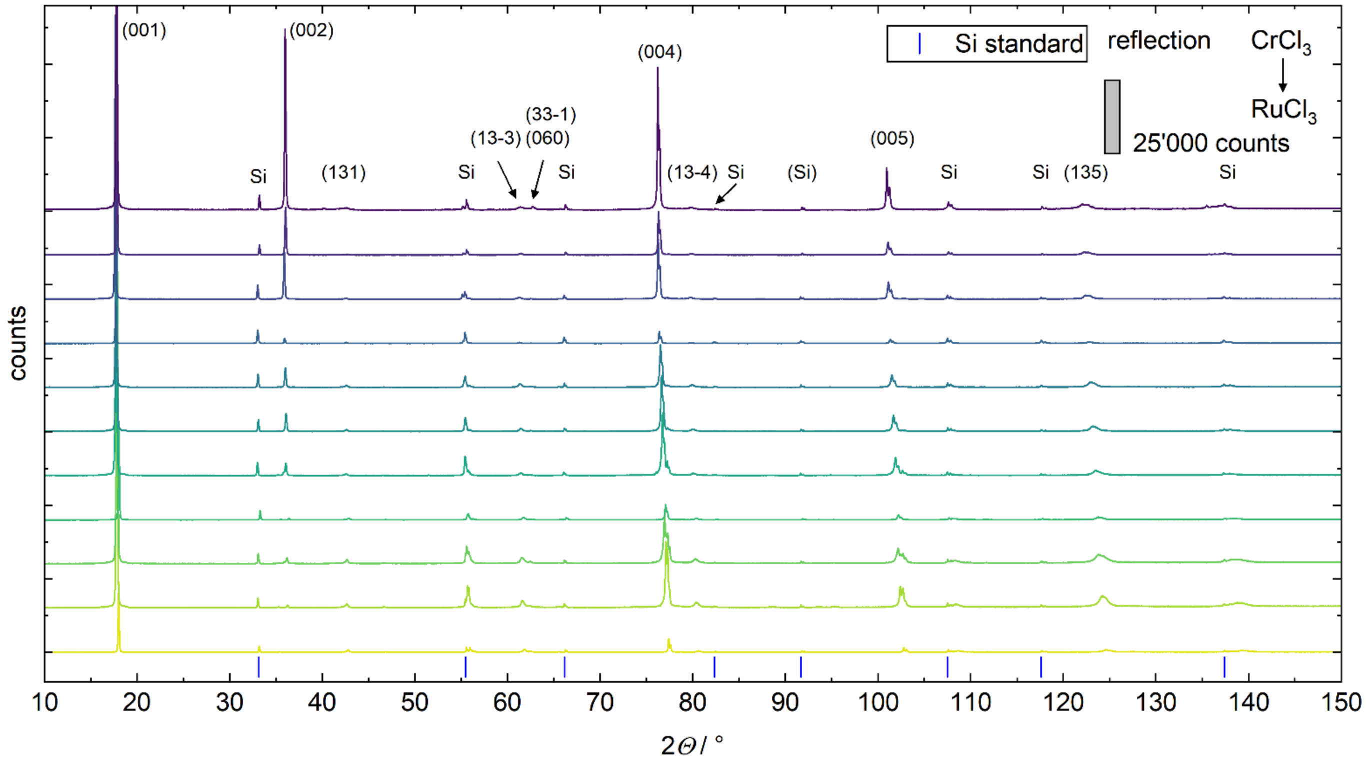

Figure S4 – Unmanipulated, stacked powder XRD pattern of the $Cr_{1-x}Ru_xCl_3$ solid solution series in steps of 10 mol%, measured in reflection geometry. The (001) reflection (ca. 18 °) not entirely shown due to visibility of the other reflexes. The counts for these reflections range between 198000 for $CrCl_3$ and 17000 for $x = 0.7$.

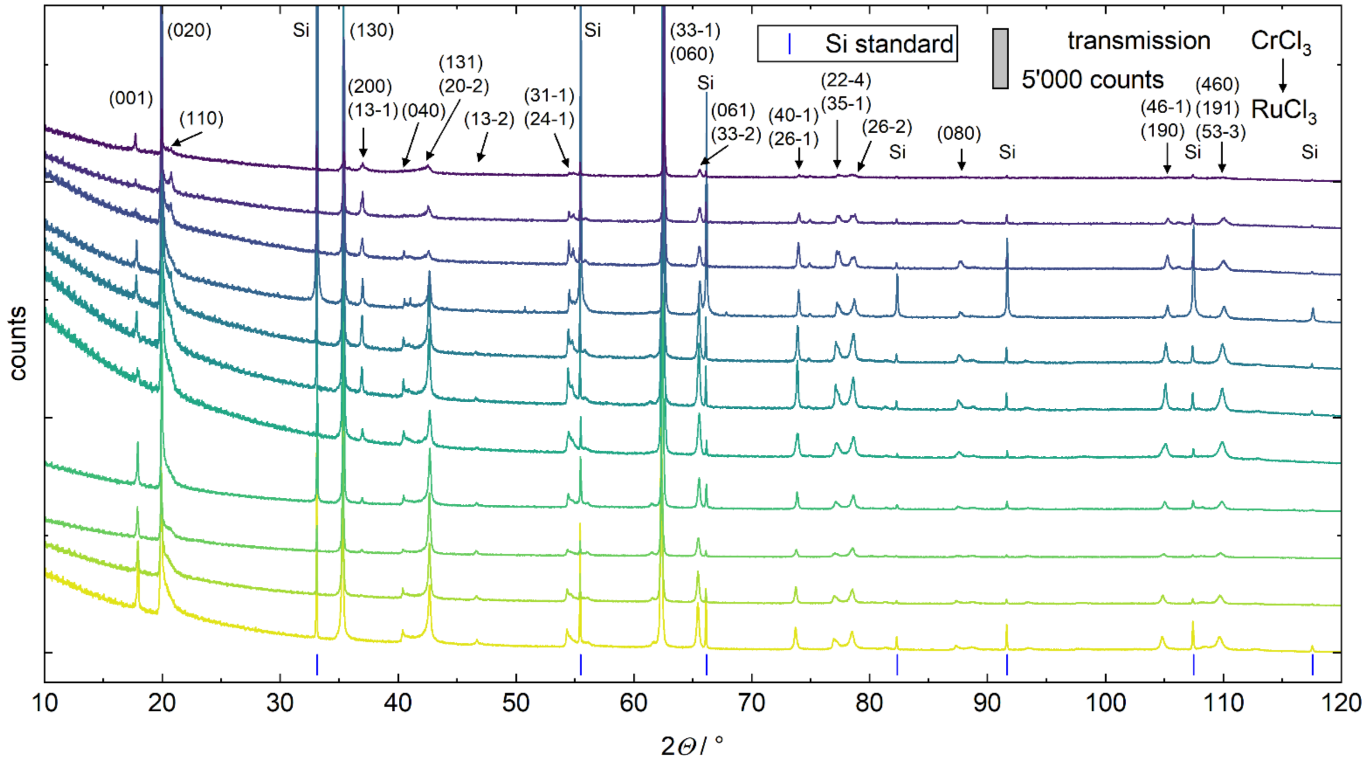

Figure S5 – Unmanipulated, stacked powder XRD pattern of the $Cr_{1-x}Ru_xCl_3$ solid solution series in steps of 10 mol%, measured in transmission geometry. The (002) (ca. 20 °), (130) (ca. 35 °) and (060) (ca. 62 °) reflections of solid solution, as well as (111) (33 °) and (220) (55 °) reflections of Si standard not entirely shown due to visibility of the other reflexes. The sample with 70 % $CrCl_3$ contains significantly more Si-standard compared to the other samples, thus the intensity of the Si reflections is proportionally larger.

Table S4 – Results of the EDX measurements for the enrichment experiments with different starting compositions and temperatures. For each experiment 5 different crystals on the substrate were analysed and the results averaged for a total value.

			x on substrate						
		Experiment	1	2	3	4	5	$\bar{x}$	$s(\bar{x})$
x = 0.1	575 °C ⇨ 525 °C	1	0.074	0.069	0.071	0.062	0.074	0.070	0.0051
		2	0.060	0.061	0.092	0.077	0.062	0.070	0.0140
	650 °C ⇨ 600 °C	1	0.103	0.023	0.024	0.042	0.049	0.048	0.0328
		2	0.043	0.052	0.060	0.046	0.055	0.051	0.0069
x = 0.2	575 °C ⇨ 525 °C	1	0.107	0.166	0.124	0.139	0.121	0.131	0.0223
		2	0.102	0.145	0.064	0.163	0.107	0.116	0.0388
	650 °C ⇨ 600 °C	1	0.079	0.031	0.059	0.062	0.134	0.073	0.0383
		2	0.071	0.093	0.090	0.090	0.103	0.090	0.0116
x = 0.3	575 °C ⇨ 525 °C	1	0.150	0.149	0.173	0.161	0.152	0.157	0.0103
		2	0.151	0.150	0.137	0.157	0.148	0.149	0.0075
	650 °C ⇨ 600 °C	1	0.153	0.160	0.163	0.192	0.174	0.168	0.0150
		2	0.144	0.169	0.172	0.150	0.139	0.155	0.0152
x = 0.4	575 °C ⇨ 525 °C	1	0.136	0.147	0.157	0.139	0.142	0.144	0.0083
		2	0.146	0.158	0.163	0.147	0.160	0.155	0.0078
	650 °C ⇨ 600 °C	1	0.168	0.164	0.157	0.112	0.141	0.149	0.0226
		2	0.144	0.150	0.171	0.156	0.214	0.167	0.0281
x = 0.5	575 °C ⇨ 525 °C	1	0.341	0.311	0.343	0.370	0.291	0.331	0.0307
		2	0.325	0.291	0.341	0.368	0.311	0.327	0.0292
	650 °C ⇨ 600 °C	1	0.349	0.342	0.348	0.349	0.368	0.351	0.0098
		2	0.311	0.353	0.318	0.344	0.350	0.335	0.0193
x = 0.6	575 °C ⇨ 525 °C	1	0.253	0.274	0.336	0.343	0.334	0.308	0.0416
		2	0.299	0.336	0.305	0.311	0.330	0.316	0.0162
	650 °C ⇨ 600 °C	1	0.402	0.417	0.409	0.395	0.357	0.396	0.0232
		2	0.366	0.377	0.448	0.403	0.385	0.396	0.0322
x = 0.7	575 °C ⇨ 525 °C	1	0.383	0.375	0.343	0.370	0.333	0.361	0.0215
		2	0.458	0.480	0.484	0.475	0.497	0.479	0.0145
	650 °C ⇨ 600 °C	1	0.536	0.580	0.487	0.505	0.573	0.536	0.0409
		2	0.461	0.516	0.544	0.511	0.587	0.524	0.0461
x = 0.8	575 °C ⇨ 525 °C	1	0.521	0.548	0.609	0.635	0.591	0.581	0.0459
		2	0.585	0.537	0.507	0.532	0.521	0.536	0.0296
	650 °C ⇨ 600 °C	1	0.735	0.692	0.660	0.670	0.722	0.696	0.0324
		2	0.670	0.661	0.727	0.674	0.653	0.677	0.0292
x = 0.9	575 °C ⇨ 525 °C	1	0.808	0.817	0.852	0.845	0.873	0.839	0.0265
		2	0.861	0.861	0.850	0.858	0.827	0.851	0.0144
	650 °C ⇨ 600 °C	1	0.875	0.886	0.884	0.884	0.892	0.884	0.0060
		2	0.853	0.849	0.854	0.854	0.848	0.852	0.0030

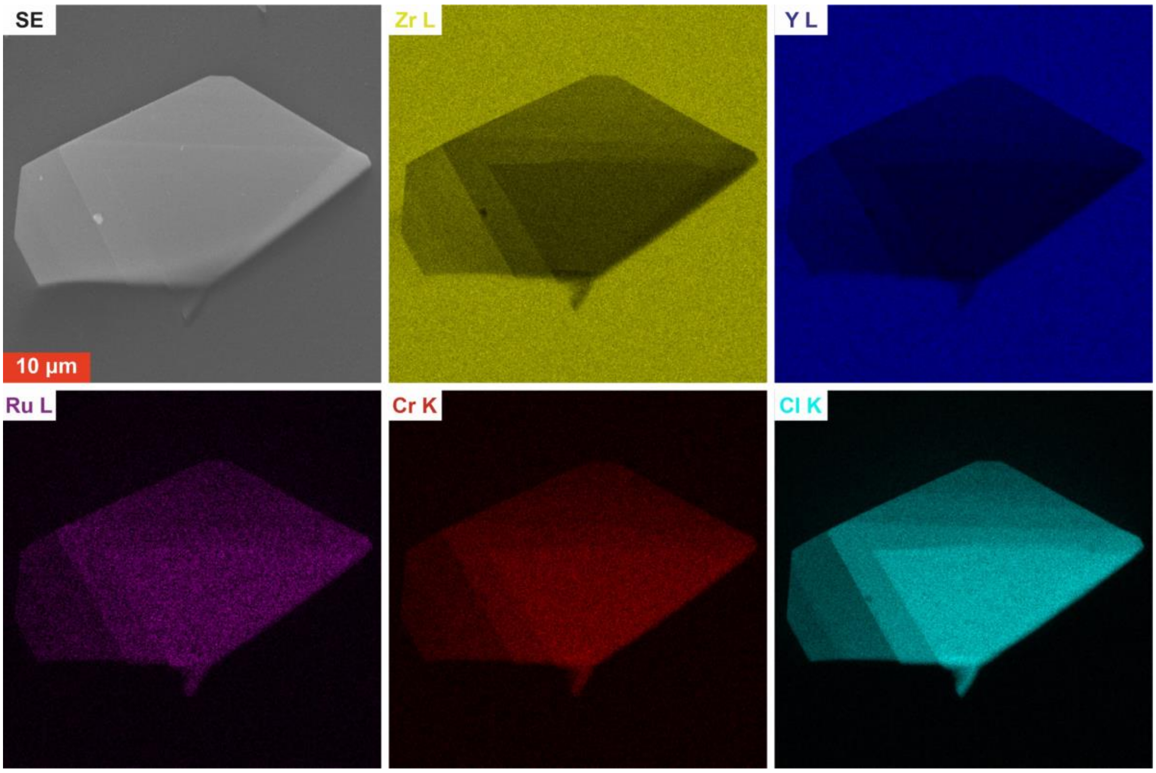

Figure S6 – Secondary electron image and EDX mapping of relevant elements of an as-grown solid solution nanocrystal. Ru and Cr show a homogeneous distribution inside the crystal. EDX signals of Zr and Y in the area of the nanocrystal arise from the thinness of crystal, so that the substrate background is still detectable by EDX at 15 kV acceleration voltage.

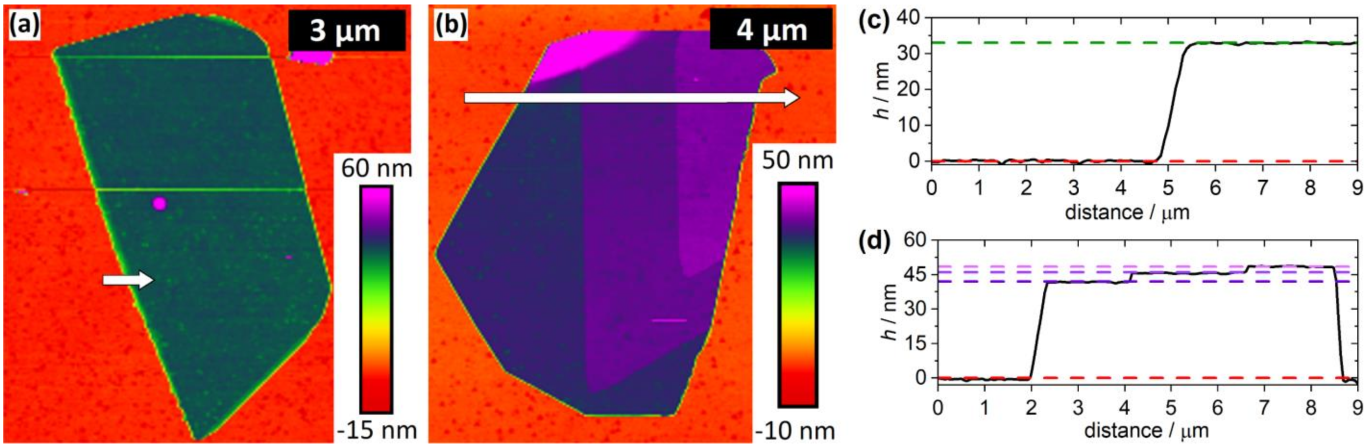

Figure S7 – AFM images of as-grown nanocrystals with (a) flat surface (line artefacts come from high particles next to the crystal) and (b) additional layer steps on top and a bended corner. White arrows indicate the line scan direction shown in (c) and (d), which belong to (a) and (b) respectively.

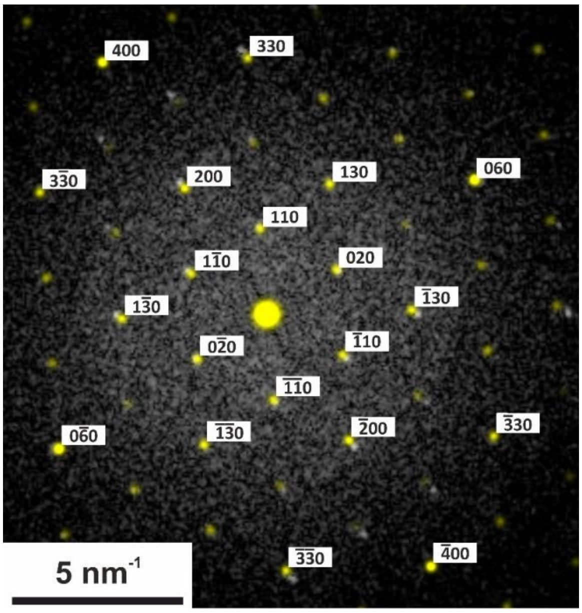

Figure S8 – Fourier transformed image as in Figure 6 (c) of the main article (white spots), overlaid with the simulated diffraction pattern for a composition of *x* = 0.4 (yellow spots). Most of the experimental reflections are covered by the simulated ones.

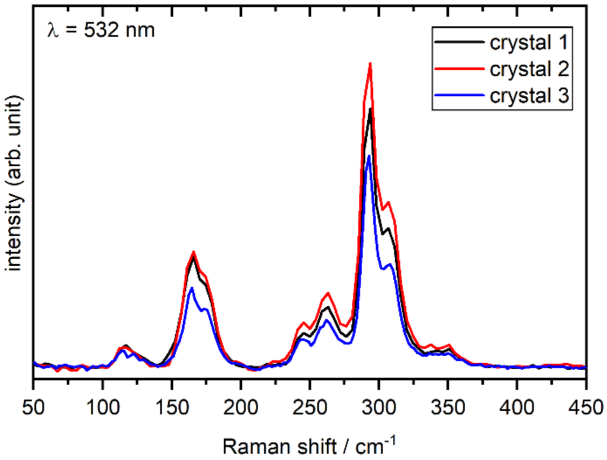

Figure S9 – Raman spectra of three different crystals on the same substrate. No peak shifts are visible, indicating equal Cr : Ru ratios.

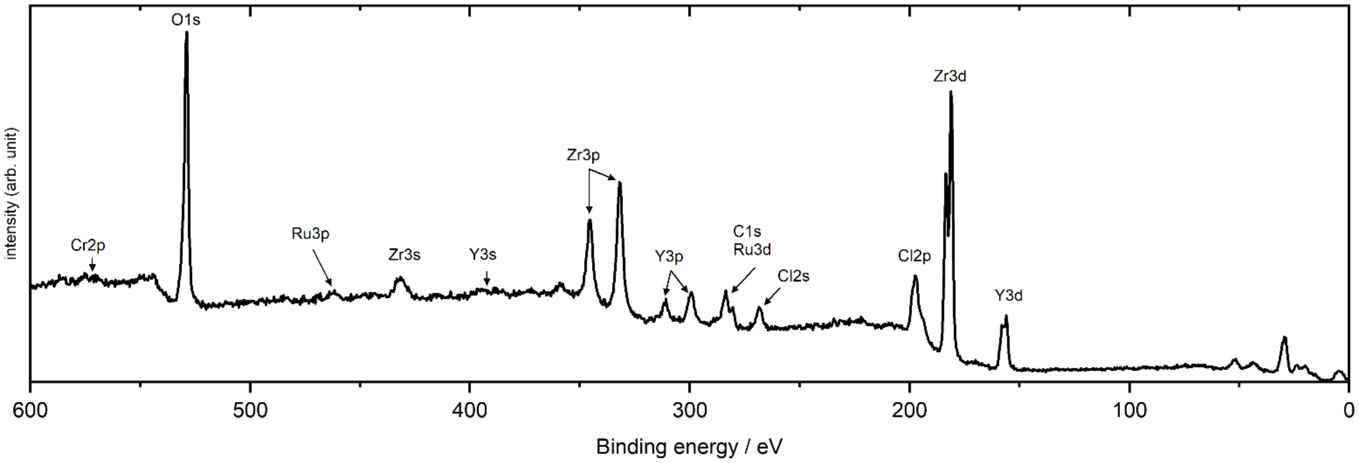

Figure S10 – Relevant section of the XPS survey of a YSZ substrate with deposited crystals of *x* = 0.4.

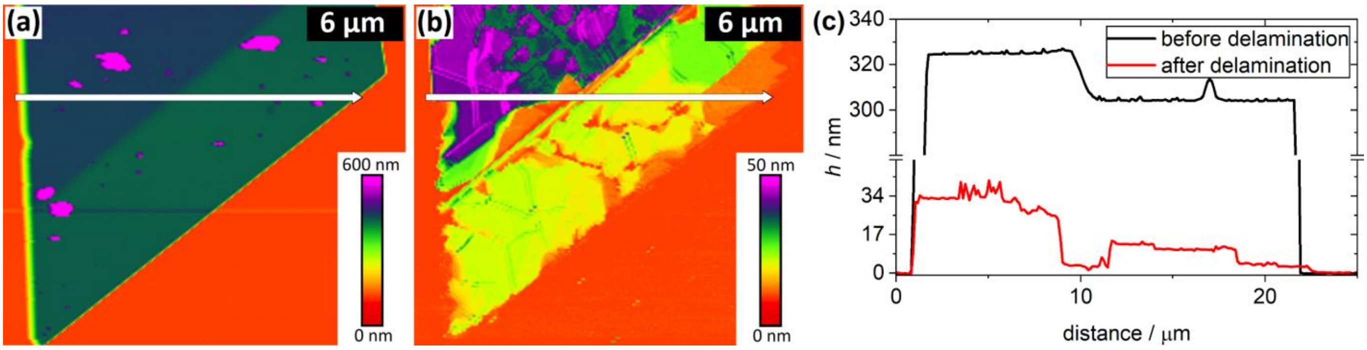

Figure S11 – AFM image of nanocrystals (a) before delamination, (b) after delamination by ultrasound in NMP for 2 minutes with drastically reduced height. (c) Comparison of the height profiles of the nanocrystals shown in (a) and (b), indicated there by the white arrow.

References

1 G. Krabbes, W. Bieger, K.-H. Sommer, T. Söhnel and U. Steiner, *TRAGMIN 5.1*, Dresden, 2014.

2 G. Krabbes, W. Bieger, K.-H. Sommer and E. Wolf, *J. Cryst. Growth*, 1991, **110**, 433–444.

3 K. Nocker and R. Gruehn, *Z. Anorg. Allg. Chem.*, 1993, **619**, 699–710.

4 J. A. Rard, *Chem. Rev.*, 1985, **85**, 1–39.

5 J. Feller, Dissertation, TU Dresden, 1996.

6 C. W. Bale, E. Bélisle, P. Chartrand, S. A. Decterov, G. Eriksson, A. E. Gheribi, K. Hack, I. H. Jung, Y. B. Kang, J. Melançon, A. D. Pelton, S. Petersen, C. Robelin, J. Sangster, P. Spencer and M. A. Van Ende, *Calphad*, 2016, **54**, 35–53.